

SUPPORTING INFORMATION

Oxygen Vacancy Linear Clustering

in a Perovskite Oxide

Kitae Eom[†], Euiyoung Choi[†], Minsu Choi[†], Seungwu Han[‡], Hua Zhou[§], and Jaichan Lee^{*†}

[†]School of Advanced Materials Science and Engineering, Sungkyunkwan University, Suwon 16419, Korea,

[‡]Department of Materials Science and Engineering, Seoul National University, Seoul 08826, Korea

[§]Advanced Photon Source, Argonne National Laboratory, Argonne, Illinois 60439, United States

*E-mail: jclee@skku.edu (Jaichan Lee)

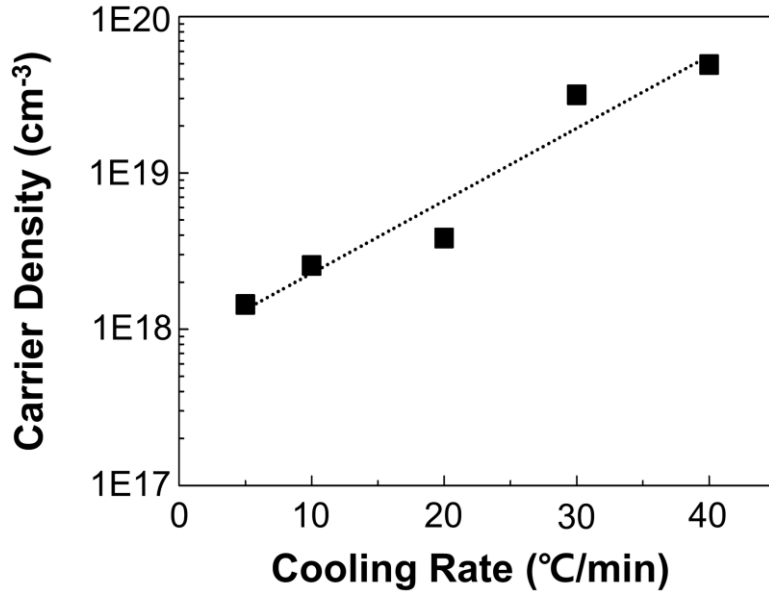


Figure S1. Carrier density of SrTiO_{3-δ} thin films cooled at different cooling rates. The cooling process was performed at the same as the deposition pressure. The carrier density decreased with decreasing the cooling rate, indicating that fast cooled films become highly oxygen deficient.

A. Divacancy model and estimation of crossover temperature

We estimated the crossover temperature (T_{cr}) using a divacancy cluster model. In the model, the change in the free energy ΔF_1 and ΔF_2 of the oxygen-deficient SrTiO₃ containing isolated oxygen vacancies and divacancies per unit cell, respectively, from the perfect crystal are expressed by the following relations:

$$\Delta F_1 = (\delta m E_0 - k_B T \ln \Omega_1) / m$$

$$\Delta F_2 = [\delta m / 2 (2E_0 - \varepsilon) - k_B T \ln \Omega_2] / m \quad (\text{Eq. S1})$$

where m is the number of unit cell in SrTiO₃, δ is the concentration of the oxygen vacancy deficiency, ε is the interaction energy (or binding energy) of two oxygen vacancies in a

divacancy form, E_0 is the internal energy of the isolated oxygen vacancy, and Ω is the number of configurations of the isolated oxygen vacancies or divacancies in the oxygen lattice sites of m unit cells. The binding energy was first estimated from the Maxwell-Boltzmann distribution. Assuming that the low temperature annealing induces the dimerization of oxygen vacancies accompanied by electron localization, the carrier density n is determined by the relative concentration of the oxygen vacancy in the isolated and divacancy forms.

$$n/n_0 \propto N_{V_{2O}}/N_{V_O} \propto \exp[-(\Delta F_2 - \Delta F_1)/k_B T] \quad (\text{Eq. S2})$$

N_{V_O} and $N_{V_{2O}}$ are the concentrations of the isolated and divacancy, respectively. Then the carrier density follows the change of the relative concentration of the oxygen vacancy and, using the Eq. (S1), is expressed as follows:

$$n/n_0 \propto \exp(-\delta\varepsilon/2k_B) \quad (\text{Eq. S3})$$

Here, n_0 and δ were estimated to be 0.04 from the Hall carrier density of the fast cooled $\text{SrTiO}_{3-\delta}$ thin films. The interaction energy ε of 0.35 eV was obtained from the extrapolation of the carrier density change at low temperatures (inset of Fig. 2).

T_{cr} was also estimated from the interaction energy obtained in the model. The isolated vacancies and divacancy are equilibrated at T_{cr} with the condition: $\Delta F_1 = \Delta F_2$. The configuration entropies in the free energy expressions are approximated by Stirling formula as follows:

$$\Omega_1 = \left[\frac{(3n)!}{(3n-\delta n)!(\delta n)!} \right], \quad \Omega_2 = \left[\frac{(n)!}{(n-\delta n/2)!(\delta n/2)!} \right] \quad (\text{Eq. S4a})$$

$$\ln \Omega_1 = \left[3 \ln \left(\frac{3}{3-\delta} \right) + \delta \ln \left(\frac{3}{\delta} - 1 \right) \right], \ln \Omega_2 = \left[\ln \left(\frac{2}{2-\delta} \right) + \frac{\delta}{2} \ln \left(\frac{2}{\delta} - 1 \right) \right], \quad (\text{Eq. S4b})$$

The free energy of the oxygen-deficient SrTiO₃ containing isolated oxygen vacancies and divacancies per unit cell can be expressed by substituting the number of configurations (Ω) into Eq. S1.

$$\Delta F_1 = \left[\delta m E_0 - K_B T \left\{ 3 \ln \left(\frac{3}{3-\delta} \right) + \delta \ln \left(\frac{3}{\delta} - 1 \right) \right\} \right] / m \quad (\text{Eq. S5a})$$

$$\Delta F_2 = \left[\delta m / 2 (2E_0 - \varepsilon) - K_B T \left\{ \ln \left(\frac{2}{2-\delta} \right) + \frac{\delta}{2} \ln \left(\frac{2}{\delta} - 1 \right) \right\} \right] / m \quad (\text{Eq. S5b})$$

From the equilibrium condition ($\Delta F_1 = \Delta F_2$), the cross-over temperature is obtained as a function of the oxygen deficiency δ by the following equation:

$$T_{cr}(\delta) = \frac{\varepsilon}{k_B} \frac{\delta}{2} \left[3 \ln \left(\frac{3}{3-\delta} \right) + \delta \ln \left(\frac{3}{\delta} - 1 \right) - \ln \left(\frac{2}{2-\delta} \right) - \frac{\delta}{2} \ln \left(\frac{2}{\delta} - 1 \right) \right]^{-1} \quad (\text{Eq. S6})$$

T_{cr} obtained from Eq. (S6) is 437 °C, in good agreement with the cross-over temperature (440 °C) obtained from the carrier density measurement, as shown in Fig. 2.

B. Photoemission spectroscopy.

In photoemission, electron emission is influenced by the roughness as well as contamination of a sample surface. Therefore, sputtering is often followed by annealing to make the surface smooth because sputtering can cause a rough surface. In our approach, however, the thermal

treatment would affect Ti valence state of the sample, especially Ti^{2+} state which is a good indicator of the oxygen vacancy clustering. Thus, sputtering without annealing treatment was carried out to clean the sample surface not to induce nonstoichiometry at the sample surface. The roughness of a sample surface before and after the sputtering was examined by atomic force microscopy and compared to investigate the effect of the sputtering on the sample surface (Figure S2). The roughness of the sample surface was little changed by the sputtering and the surface remained smooth (within an *rms* roughness of 0.4 nm). The effect of the roughness on the intensity of XPS signals has been studied both experimentally and theoretically.^{1,2} The XPS signal intensities from a rough and smooth surface were very similar, provided that both surfaces were clean and no shading effect occurred. The photoemission process is influenced by surface roughness when escaping electrons are shaded by adjacent rough surface.³ Thus emission angle can be a crucial factor in alleviating the influence of the surface roughness. The influence of surface roughness on photoelectron intensity was investigated by angle-resolved photoelectron spectroscopy.⁴ Two silicon surfaces with different roughness, i.e., *rms* of 4.9 nm and 6.3 nm were examined by changing an emission angle. The difference in the photoelectron intensities from two surfaces was large at low emission angles and decreased with increasing the emission angle. When the emission angle reached 90° , surface roughness rarely influenced the photoelectron intensities due to minimizing shading effect. Our sample surfaces were not only quit smooth compared with the previous cases, but also the spectrum was acquired at a normal emission ($\theta=90^\circ$). Thus, our XPS results will not be influenced by sputtering. Furthermore, the signal detection at the normal emission helps probing the samples into deeper region from a surface.

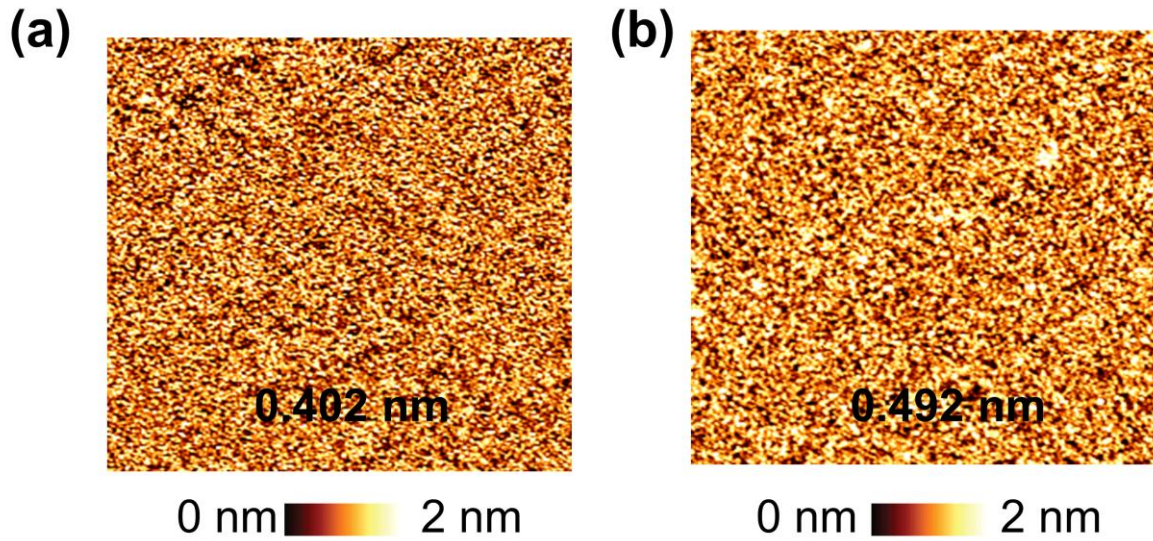


Figure S2. The AFM images were acquired after measuring PES. The samples treated at different annealing conditions: (a) fast-cooled film (b) annealed at 250 °C 60 min. The RMS surface roughness was nearly identical for samples tested, indicating that the sample surfaces remain quit smooth after the sputtering treatment.

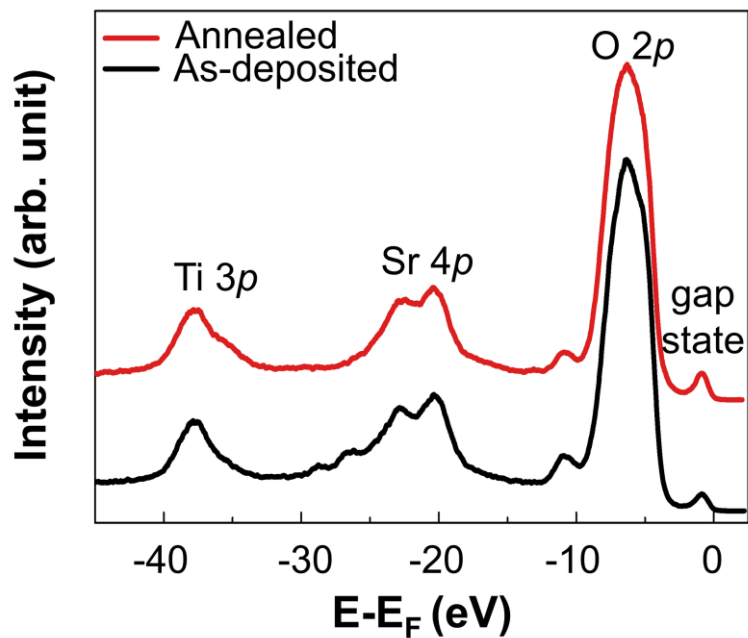


Figure S3. PES spectra of fast-cooled and annealed $\text{SrTiO}_{3-\delta}$ thin films at 250°C/60 min (shown as black and red lines). A gap-state is also shown above the O 2p band.

C. X-ray diffuse scattering characterizations

In order to characterize possible oxygen vacancy clustering in oxygen deficient $\text{SrTiO}_{3-\delta}$, we have performed synchrotron X-ray diffuse scattering measurements. As demonstrated in Figure 4, K - L and H - L 2D cross-section view presented the primary Bragg peak (-101) and the surround diffuse scattering. The extended circular pattern indicated the modest crystallographic mosaicity of annealed $\text{SrTiO}_{3-\delta}$ thin film. Another distinct features in both 2D views are the line-shape patterns horizontally extending across both H and K directions, which suggested a planar feature in the 3D reciprocal space volume. A 2D planar feature in reciprocal space can be attributed to a 1D type of line defects along certain crystallographic orientation in real space, which is in line with the linear clustering of oxygen vacancy inside $\text{SrTiO}_{3-\delta}$ thin film. On the other hand, the as-grown films do not show the linear feature (Figure S4). Although several lines are seen in the 2D maps, they are image artifacts due to X-ray photon sensor chips of local discontinuity. The X-ray detector used is a 2D pixel array X-ray photon counting detector. The whole detector is composed of a set of small sensor chips and there are small physical gaps. These gap patterns can be observed as linear features on X-ray exposure. On the other hand, several tests on the annealed films confirmed the linear feature in 2D maps.

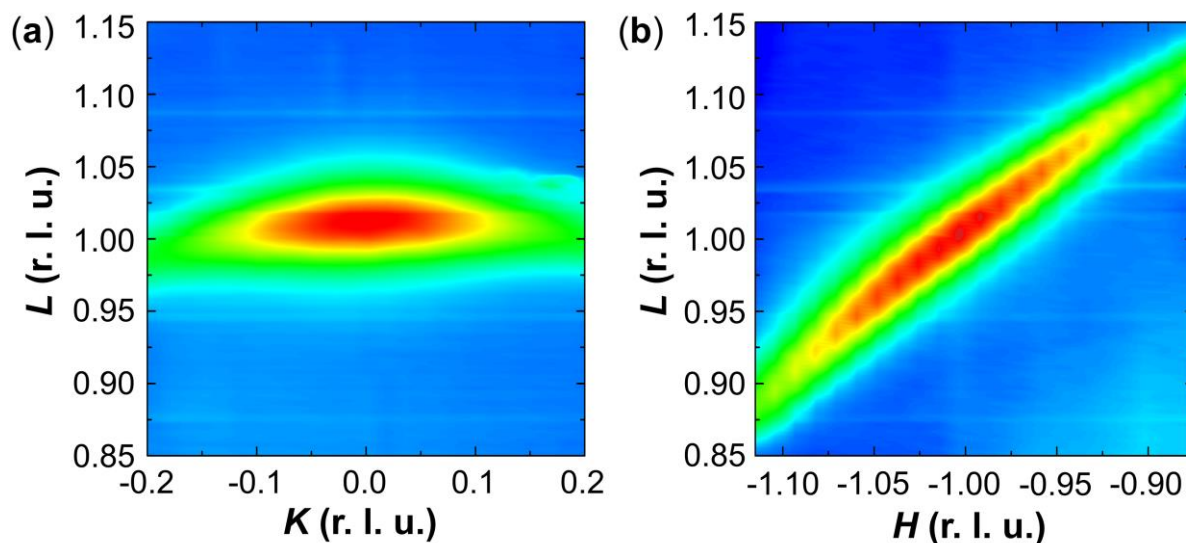


Figure S4. X-ray diffuse scattering (a) 2D K - L and (b) H - L views around (-101) Bragg peak of an as-grown $\text{SrTiO}_{3-\delta}$ thin film.

Reference

- (1) Gunter, P. L. J.; Gijzeman, O. L. J.; Niemantsverdriet, J. W. Surface Roughness Effects in Quantitative XPS: Magic Angle for Determining Overlayer Thickness. *Appl. Surf. Sci.* **1997**, *115*, 342-346.
- (2) Fadley, C. S. Instrumentation for Surface Studies: XPS Angular Distributions. *J. Electron Spectrosc. Relat. Phenom.* **1974**, *5*, 725-754.
- (3) Fadley, C. S.; Baird, R. J.; Siekhaus, W.; Novakov, T.; Bergstrom, S. A. L. Surface Analysis and Angular Distributions in X-ray Photoelectron Spectroscopy. *J. Electron Spectrosc. Relat. Phenom.* **1974**, *4*, 93-137.
- (4) Zemek, J.; Olejnik, K.; Klapetek, P. Photoelectron Spectroscopy from Randomly Corrugated Surfaces. *Surf. Sci.* **2008**, *602*, 1440-1446.